

# Deglacial changes in dust flux in the eastern equatorial Pacific

D. McGee<sup>a,\*</sup>,<sup>1</sup>, F. Marcantonio<sup>a,2</sup>, J. Lynch-Stieglitz<sup>b</sup>

<sup>a</sup> *Department of Earth and Environmental Sciences, Tulane University, New Orleans, LA 70118, USA*

<sup>b</sup> *School of Earth and Atmospheric Sciences, Georgia Institute of Technology, Atlanta, GA 30332, USA*

Received 21 December 2006; received in revised form 15 February 2007; accepted 16 February 2007

Available online 27 February 2007

Editor: M.L. Delaney

## Abstract

Atmospheric dust levels may play important roles in feedbacks linking continental source areas, tropical convection, marine productivity, and global climate. These feedbacks appear to be particularly significant in the tropical Pacific, where variations in local convection and productivity have been demonstrated to have impacts on climate at higher latitudes. Modeling of past dust levels and related feedbacks has been limited, however, by a paucity of observational data. In this study we present a temporal and spatial survey of dust fluxes to the eastern equatorial Pacific over the past 30 kyr. Glacial and Holocene fluxes of <sup>232</sup>Th, a proxy for continental material, were calculated by normalization to <sup>230</sup>Th from a north–south transect of cores along 110°W between 3°S and 7°N (ODP sites 848–853). Fluxes were 30–100% higher during the last glacial, suggesting increased dustiness in both hemispheres during the glacial period. In both time periods, dust fluxes decrease towards the south, reflecting scavenging of Northern Hemisphere dust by precipitation at the ITCZ. The Holocene meridional dust flux gradient between 7°N and 3°S is characterized by a steep drop in dust levels at the southern edge of the modern range of the ITCZ, while the gradient is shallower and more nearly linear during the last glacial. This change may indicate that the glacial ITCZ in this region was a less effective barrier to inter-hemispheric dust transport, most likely due to a decrease in convective intensity and precipitation during the last glacial; alternatively, the change in gradient may be explained by increased variability in the location of the glacial ITCZ. Our data do not appear to require a mean southerly displacement of the glacial ITCZ, as suggested by the results of other studies.

© 2007 Elsevier B.V. All rights reserved.

**Keywords:** dust flux; eastern equatorial Pacific; deglacial; <sup>230</sup>Th-profiling; ITCZ; ODP Leg 138

## 1. Introduction

Concentrations of mineral aerosol (dust) may form an important link in feedbacks connecting continental conditions and global climate. Models of Last Glacial Maximum (LGM; ~19–23 ka) conditions suggest that increased dust levels contributed to cooling in the tropics by increasing albedo, leading to a change in tropical radiative forcing that may have been similar in magnitude (–3 to –4 W m<sup>–2</sup>) to the effects of low atmospheric *p*CO<sub>2</sub> at the time [1]. Dust-related radiative forcing may have significantly diminished the intensity

\* Corresponding author. Lamont-Doherty Earth Observatory, Columbia University, P.O. Box 1000, Palisades, NY, 10964, USA. Tel.: +1 845 365 8569; fax: +1 845 365 8155.

E-mail addresses: [dmcgee@ldeo.columbia.edu](mailto:dmcgee@ldeo.columbia.edu) (D. McGee), [marcantonio@geo.tamu.edu](mailto:marcantonio@geo.tamu.edu) (F. Marcantonio), [jean@eas.gatech.edu](mailto:jean@eas.gatech.edu) (J. Lynch-Stieglitz).

<sup>1</sup> Present address: Lamont-Doherty Earth Observatory, Columbia University, New York, NY 10964, USA.

<sup>2</sup> Present address: Department of Geology and Geophysics, Texas A&M University, College Station, TX 77843, USA.

of tropical convection [2] and precipitation [3], potentially leading to reductions in poleward heat and moisture transport and greenhouse gas production [4]. Increased dust levels may also contribute to cooling by spurring added productivity and carbon export in high-nutrient, low-chlorophyll marine ecosystems such as the eastern equatorial Pacific (EEP) [5,6], the site of the present study.

Because of the potential importance of these and other dust-related feedbacks in amplifying global climate changes, characterization of past tropical atmospheric dust loading has repeatedly been identified as a prerequisite to more accurate modeling of past climates (e.g., [1,7]). Existing studies of tropical sediments and ice cores have established that dust flux was higher in both hemispheres during past glacial periods (e.g., [7–10]). A possible exception to this pattern is the equatorial Pacific, where a record from the EEP (DSDP 503B) indicated reduced dust flux during glacial periods, and results from the central equatorial Pacific (RC11-210) displayed no consistent climate pattern [8]. A recent study, however, found increased glacial dust flux in central equatorial Pacific cores likely to receive dust from the same sources [11], suggesting that dust deposition in the equatorial Pacific may be similar to patterns elsewhere in the world.

The number of tropical dust flux records is still small, particularly in the EEP, and even fewer of these records have carefully tracked changes in dust flux over the last deglaciation, the largest-magnitude climate change of the past 100 kyr. In this study,  $^{230}\text{Th}$ -normalized fluxes of  $^{232}\text{Th}$  were used to quantify dust fluxes from the past 30 kyr in a meridional transect of cores along  $110^\circ\text{W}$  from  $3^\circ\text{S}$  to  $7^\circ\text{N}$  (ODP sites 848–853). The data represent one of the most complete temporal and spatial surveys to date of changes in tropical dust flux during deglaciation, and together with previous results [11,12] provide a consistent picture of glacial and Holocene dust levels throughout the equatorial Pacific.

The present study area is also an ideal place to study past behavior of the Intertropical Convergence Zone (ITCZ), an area of intense convection and precipitation located at the region of maximum sea surface temperature and the meeting of the north- and southeasterly trade winds. In the Eastern Equatorial Pacific, the ITCZ ranges between  $4^\circ\text{N}$  in boreal winter and  $11^\circ\text{N}$  in boreal summer, with associated shifts in local precipitation patterns and upwelling. Changes in the convective intensity of the ITCZ may impact both greenhouse gas concentrations [4] and poleward heat and moisture

transport [13], while changes in ITCZ position have been linked to ENSO variability, thermohaline circulation intensity, marine productivity, and terrestrial aridity (e.g., [14,15]).

Several studies have suggested that the ITCZ over South America was displaced southward during the LGM (see review by Koutavas and Lynch-Stieglitz [14]). Past motions of the marine ITCZ are less well constrained, due in part to the difficulty of tracking precipitation and wind patterns in sediment records from the open ocean. In the EEP, stable isotope records indicating reduced glacial SST gradients have provided a first indication that the Pacific ITCZ moved south and experienced reduced convective intensity during the LGM [16].

Studies of eolian dust flux may assist in tracking marine ITCZ dynamics over time, as spatial patterns of dust deposition reflect trade wind and precipitation patterns [17,8]. At the ITCZ, dust is removed from the upper troposphere by deep convection and scavenged by precipitation. The ITCZ thus forms a barrier to inter-hemispheric dust transport, separating higher levels of dust in the northern hemisphere from lower dust levels in the southern hemisphere [18,8]. Sediments under the Pacific ITCZ accordingly display strong meridional gradients in dust flux [11,19,8] and provenance [20–22]. Researchers have attempted to use these changes to track past positions of the ITCZ, finding evidence for positions north of its current location during the Miocene [19,23,24]. A similar study found evidence for a southern ITCZ position in the Atlantic during the LGM, though sediment redistribution could not be ruled out as a cause of the observed glacial–interglacial changes [9]. In this study we make a first attempt to use changes in the cross-ITCZ dust flux gradient as an indicator of changes in the Pacific ITCZ during the last deglaciation.

## 2. Study area

The cores used in this study were collected during Leg 138 of the Ocean Drilling Program (ODP) and come from ODP sites 848–853. The sites lie within  $0.6^\circ$  of  $110^\circ\text{W}$  between  $3.0^\circ\text{S}$  and  $7.2^\circ\text{N}$ , forming an equator-crossing meridional transect (Fig. 1; Table 1). We also attempted to include samples from ODP site 854 ( $109.5^\circ\text{W}$ ,  $11.2^\circ\text{N}$ ), but these contained abundant volcanic glass, preventing use of  $^{232}\text{Th}$  as a proxy for eolian inputs. All cores are piston cores and contain greater than 60% carbonate, with varying amounts of biogenic silica and lithogenic material [26]. Cores from sites 848–851 were sampled at 10-cm intervals, while

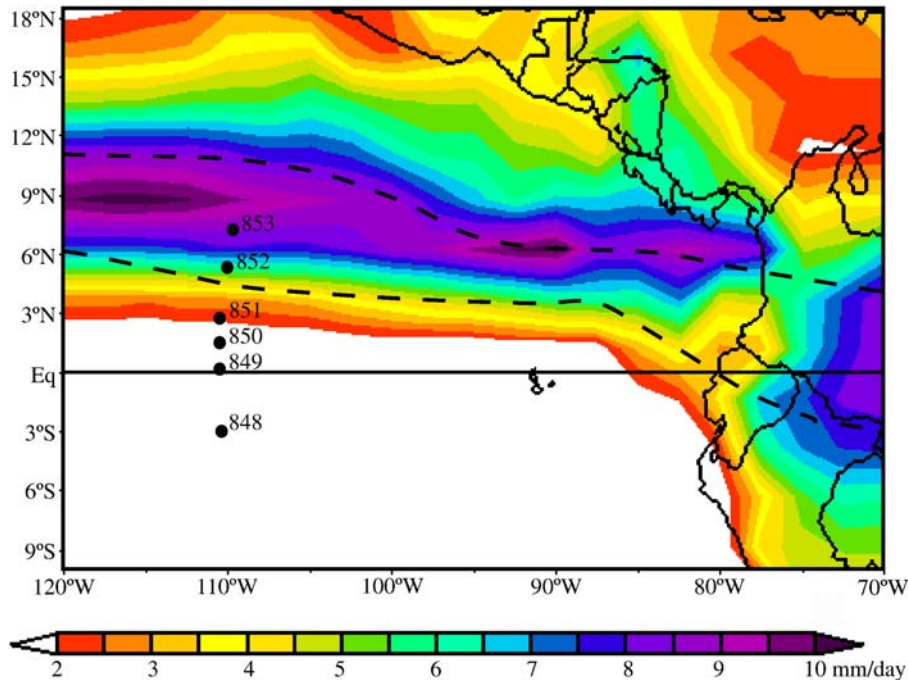


Fig. 1. Map of ODP sites used in this study and regional precipitation patterns. Long-term mean (1979–2004) Climate Prediction Center Merged Analysis of Precipitation (CMAP) annual precipitation rates are shown in colored contours [25]. The mean ITCZ position lies approximately along the region of maximum precipitation. Dotted lines show approximate August–September (top) and February–March (bottom) ITCZ positions over the same period of time. (For interpretation of the references to color in this figure legend, the reader is referred to the web version of this article.)

those from sites 852 and 853 were sampled at 5- and 3-cm intervals, respectively.

### 3. Methods

#### 3.1. Thorium and uranium isotope analytical methodology

A total of 47 samples from the six cores were analyzed for thorium and uranium isotopes by isotope dilution inductively coupled plasma mass spectrometry (ICP-MS). Samples were spiked with  $^{229}\text{Th}$  and  $^{236}\text{U}$  prior to being processed following the methods of Pourmand et al. [27]. Isotope ratio measurements were made using an Element 2 ICP-MS at the University of Southern Mississippi.

Within-run sample errors based on counting statistics were consistently less than 1% for  $^{230}\text{Th}$ ,  $^{232}\text{Th}$  and  $^{238}\text{U}$ . Four replicate samples were prepared and analyzed to estimate external reproducibility, resulting in an average error of 1.8% for  $^{230}\text{Th}$ , 1.9% for  $^{232}\text{Th}$ , and 1.5% for  $^{238}\text{U}$ . Blanks were estimated by analysis of spiked and digested samples with no sediment added. Results indicated consistent  $^{232}\text{Th}$  blanks ( $4.8 \text{ ng g}^{-1}$ ) that were significant (up to 3.5%) for samples with low Th concentrations. Blanks were insignificant for  $^{230}\text{Th}$  and  $^{238}\text{U}$ . Reported errors on concentrations reflect external

reproducibility and, for  $^{232}\text{Th}$ , an estimated 1-sigma uncertainty of 25% on the blank correction.

#### 3.2. $^{230}\text{Th}$ normalization

In the present study, mass accumulation rates (MARs) and  $^{232}\text{Th}$  fluxes were calculated using the  $^{230}\text{Th}$  profiling method.  $^{230}\text{Th}$  is produced in the water column by radioactive decay of  $^{234}\text{U}$ . Due to its high particle reactivity,  $^{230}\text{Th}$  is efficiently scavenged by particulate matter and has a short residence time in the ocean (<40 yr). The rain rate of scavenged  $^{230}\text{Th}$  is then assumed to be equal to the production rate of  $^{230}\text{Th}$  in the water column. MARs are calculated by dividing the

Table 1  
Locations and depths of cores used in this study

ODP core, section	Latitude	Longitude	Depth (m)
138-848B-1H	2.99°S	110.48°W	3853
138-849A-1H	0.18°N	110.52°W	3837
138-850A-1H	1.30°N	110.52°W	3786
138-851E-1H	2.77°N	110.57°W	3760
138-852A-1H	5.29°N	110.08°W	3860
138-853B-1H	7.21°N	109.76°W	3714

production rate of  $^{230}\text{Th}$  in the water column by concentrations of scavenged  $^{230}\text{Th}$  in the sediment:

$$\text{MAR} = \beta \cdot Z / x_s^{230}\text{Th}_o$$

where  $\beta$  is the production rate of  $^{230}\text{Th}$  in the water column,  $Z$  is the water depth, and  $x_s^{230}\text{Th}_o$  is the  $^{230}\text{Th}$  concentration corrected for decay, *in situ* production of  $^{230}\text{Th}$  from authigenic  $^{234}\text{U}$ , and detrital  $^{230}\text{Th}$  (for further explanation, see [28]).

Detrital corrections in calculating  $x_s^{230}\text{Th}_o$  are <1.5% and authigenic corrections are <0.5% in all samples. The errors associated with these corrections, including those associated with the  $^{238}\text{U}/^{232}\text{Th}$  activity ratio used (0.7), are therefore negligible. Decay corrections are larger (up to 30%), but as the samples in this study are young compared to the half-life of  $^{230}\text{Th}$  (75 kyr), even errors of several thousand years in the core chronologies would change calculated fluxes by only ~4%, which is similar to the analytical uncertainty.

We see three important reasons for using  $^{230}\text{Th}$ -normalized MARs instead of age-model based MARs in the present study. First, while age-model methods calculate MARs only between dated horizons,  $^{230}\text{Th}$ -normalization provides a MAR for each sample. Second,  $^{230}\text{Th}$ -derived MARs are not dependent on the age model and its associated errors, nor do these values rely on dry bulk density data. Third,  $^{230}\text{Th}$ -derived MARs may more accurately reflect vertical inputs from the overlying water column than do age model-based MARs, which reflect the sum of inputs from all sedimentary processes. As scavenged  $^{230}\text{Th}$  travels with sediments, normalization to  $x_s^{230}\text{Th}_o$  accounts for input or removal of sediment from core sites by lateral advection and downslope transport (sediment focusing) [28]. Several studies in the equatorial Pacific have documented evidence of sediment redistribution; seismic studies commonly find accumulation enhanced by a factor of two in local depressions [29], and evidence such as scoured regions and sand waves indicates more extensive transport on steep slopes [30]. As age model-based MARs do not account for focusing, they may poorly reflect vertical fluxes. For instance,  $^{230}\text{Th}$ -based MARs for two EEP cores separated by only 10 km (Y69-71 and ME0005-24) differ by <30%, as would be expected given their proximity; age model-based MARs for these cores differ by as much as a factor of 3, suggesting that these MARs do not accurately reflect vertical fluxes and are affected by differences in focusing [30].

The  $^{230}\text{Th}$  profiling method can also be used to determine focusing factors, which indicate the fraction

of sediment added to or removed from a core by lateral redistribution. Focusing factors are expressed as the ratio of total flux to the vertical flux of sediment; factors greater than 1 indicate net focusing, while factors less than 1 indicate net winnowing. The calculation involves dividing the total inventory of  $x_s^{230}\text{Th}_o$  in a depth range in the sediment by the amount produced in the overlying water column during the corresponding period of time (see [28]). Unlike  $^{230}\text{Th}$ -normalized fluxes, the focusing factor is dependent on the age model, and so is subject to errors in the relative ages of samples. Dry bulk density, which is also used in focusing factor calculations, was estimated using existing data for companion ODP cores at these sites [31,26].

The accuracy of  $^{230}\text{Th}$ -normalized fluxes depends on two assumptions: 1) that the production of  $^{230}\text{Th}$  in the water column is equal to the flux of scavenged  $^{230}\text{Th}$  to the underlying sediments, and 2) that scavenged  $^{230}\text{Th}$  concentrations are constant across particle grain sizes. Disagreement exists over the accuracy of these approximations in the equatorial Pacific due to the divergent conclusions reached in previous paleoflux studies employing different methods of calculating MARs [32,33]. In the following, we use available evidence to constrain the accuracy of  $^{230}\text{Th}$ -normalized fluxes in our study area.

With respect to the first assumption, it has been suggested that dissolved  $^{230}\text{Th}$  is preferentially scavenged in regions of high particle flux, leading to significant underestimation of MARs and overestimation of the effects of focusing at the equator [33]. Sediment trap data [34,35] and modeling studies ([36]; M. Siddall, pers. comm.) have been used to place bounds on the effects of particle flux differences on the accuracy of  $^{230}\text{Th}$ -normalized fluxes. Both of these independent means have found that fluxes of  $x_s^{230}\text{Th}$  fall within 30% of water column production in most of the open ocean, including the present study area. Sediment trap data are a somewhat imperfect means of measuring  $x_s^{230}\text{Th}$  flux to sediments, as traps with short deployments are affected by seasonal particle flux differences that are averaged out in sediments, and shallow traps have problems with efficiency. Even so, taking uncorrected data from all open ocean traps deployed for >250 days in the Atlantic, Pacific, and Indian Oceans reported by Yu et al. [35] and Scholten et al. [34] and averaging the  $x_s^{230}\text{Th}$  fluxes for the deepest trap at each site, we calculate an average  $x_s^{230}\text{Th}$  flux/production ratio of  $0.94 \pm 0.25$ . There is also no relationship between  $x_s^{230}\text{Th}$  flux and annual average particle flux in these data, despite particle flux differences between sites of >500%. By comparison, organic carbon fluxes along

our transect differ by only  $\sim 50\%$ , so there are not likely to be large differences in  $^{230}\text{Th}$  scavenging efficiency at our sites [37].

In addressing the second assumption above, we must consider the possibility that  $^{230}\text{Th}$  is preferentially scavenged by fine particles. If this were the case, small lateral additions of  $x_s^{230}\text{Th}$ -enriched fine particles could cause significant sedimentary  $x_s^{230}\text{Th}$  increases without proportional increases in sediment accumulation, leading to an underestimation of MARs and an overestimation of focusing. An important indication that this is not the case is the agreement of equatorial Pacific  $^{230}\text{Th}$ -normalized fluxes with fluxes derived by normalization to extraterrestrial  $^3\text{He}$ , a constant flux proxy with an independent source term [38,39]. Recent results indicate that  $>70\%$  of extraterrestrial  $^3\text{He}$  is in the  $>13\ \mu\text{m}$  portion of the sediment [40]. If significant grain size fractionation of  $x_s^{230}\text{Th}$  occurred, we would expect to see the  $x_s^{230}\text{Th}$ - $^3\text{He}$  agreement break down at higher levels of focusing. Further evidence that  $x_s^{230}\text{Th}$  is not significantly enriched in the fine fraction is given by Francois et al. [32].

Lyle et al. [33] point out that focusing factors estimated by seismic profiles and sediment core comparisons in the EEP are consistently lower than those resulting from  $^{230}\text{Th}$  profiling, and suggest that the high  $^{230}\text{Th}$ -based focusing factors indicate that one or both of the above assumptions is not valid in the EEP. It is important to note, however, that focusing factors computed from seismic surveys and core comparisons are indicators of relative differences in focusing between cores; they can only be considered absolute focusing factors if the profiled area is assumed to be a closed system with respect to sedimentation. Recent studies have presented evidence that this closed-system assumption is not likely to be valid in the region surveyed by Lyle et al. [33] and have demonstrated consistency between these relative focusing factors and ratios of absolute  $^{230}\text{Th}$ -derived focusing factors for the same cores [32,30].

Models that closely replicate observed water column  $^{230}\text{Th}$  distributions indicate that  $^{230}\text{Th}$ -normalized MARs are accurate to within 10% for the four sites north of  $1^\circ\text{N}$  (850–853), and that MARs at the two southern sites may be underestimated by 15–20% due to particle flux effects ([36]; M. Siddall, pers. comm.). This uncertainty between core sites is small compared to uncertainties associated with core-to-core differences in focusing (often  $\sim 100\%$ ; [30,29]) and the time elapsed between samples in age model-based MARs (up to 100%; [30]). It is also small compared to the magnitude of the  $^{232}\text{Th}$  flux differences upon which this study's

conclusions are based; meridional differences in  $^{232}\text{Th}$  flux are 100–200% along the transect, and glacial–Holocene differences at sites 848–851 are 75–100%. The glacial–Holocene differences at sites 852 and 853 are smaller (25 and 15%, respectively); we place less confidence in these differences but still believe them to be significant.

As an independent test of our  $^{230}\text{Th}$ -normalized MARs, we note that the primary conclusions of the present study would pertain even if age model-based MARs were used. Age model-based average  $^{232}\text{Th}$  fluxes (0–20 ka) are not substantially different from those used in the study ( $\leq 30\%$ ) and show the same meridional pattern, though  $^{230}\text{Th}$ -derived average fluxes show greater internal consistency. Age-model derived  $^{232}\text{Th}$  fluxes also show approximately the same magnitude of glacial–Holocene  $^{232}\text{Th}$  flux differences.

### 3.3. Oxygen isotope analytical methodology and age models

Eight to ten specimens of *Globigerinoides sacculifer* were picked per sample for oxygen isotope analysis. When possible, all specimens came from the size fraction between 355 and 425  $\mu\text{m}$ , with smaller specimens used only in samples with low abundance. Data were acquired using a Micromass Isoprime mass spectrometer with Multiprep at the Georgia Institute of Technology. Replicate analyses of NBS-19 run concurrently with these samples had a standard deviation of 0.09‰ ( $1\sigma$ ).

The LGM is identifiable as a clear maximum in  $\delta^{18}\text{O}$  in all sites except 848 (Fig. 2). At site 853, the amplitude of the LGM–Holocene change is substantially reduced, suggesting smoothing of the gradient by bioturbation (see Section 3.4). Higher SSTs and lower salinities close to the ITCZ cause  $\delta^{18}\text{O}$  values to be depleted by up to 1‰ at the northern sites relative to the southern sites. As a result of the ambiguity of the oxygen isotope record from site 848, we instead used the coretop (0–39 ka) linear sedimentation rate (LSR) from Shackleton et al. [41] of  $1.7\ \text{cm kyr}^{-1}$  to calculate sample ages. LSRs calculated from the oxygen data for the rest of the cores are consistent with those of Shackleton et al. [41], with the exception of the LSR at site 853 (0.75 vs.  $0.4\ \text{cm kyr}^{-1}$ ). This disagreement is not unexpected given that the first datum in the existing age model is at 473 ka. Our LSRs decline with increasing distance from the equator, from a maximum of  $3\ \text{cm kyr}^{-1}$  at site 849 ( $0.2^\circ\text{N}$ ) to a minimum of  $0.75\ \text{cm kyr}^{-1}$  at site 853 ( $7.3^\circ\text{N}$ ).

Core chronologies were interpolated after location of the LGM in each core assuming a constant LSR. Several

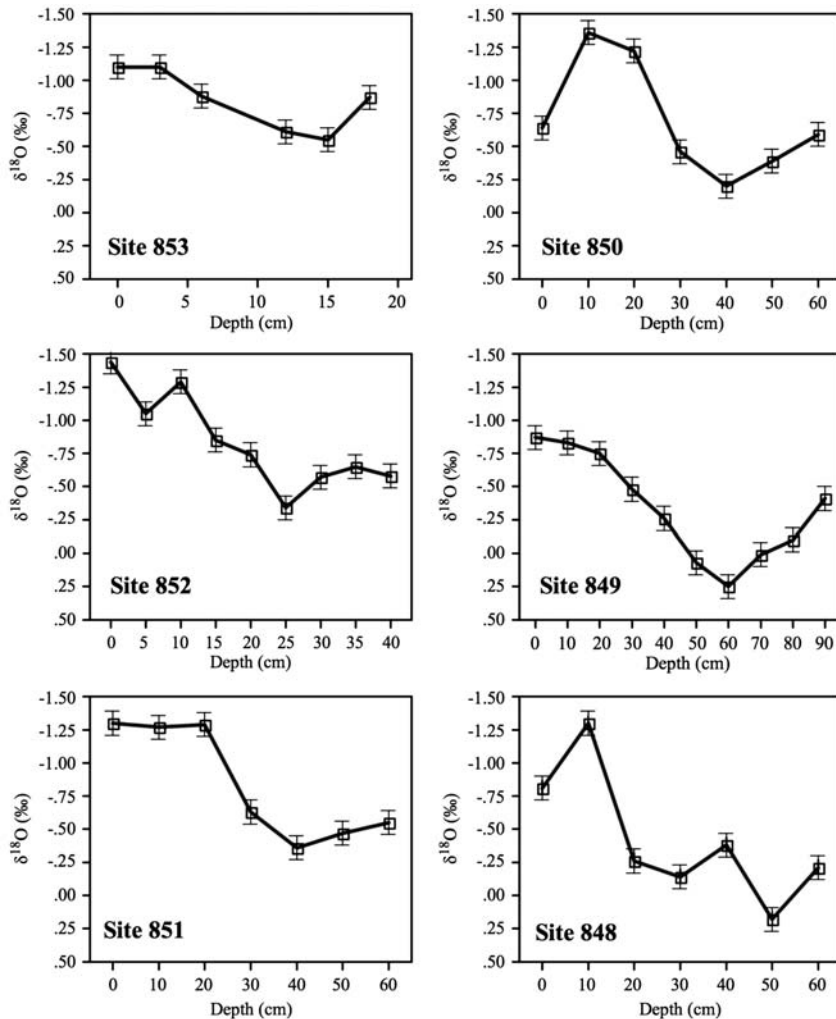


Fig. 2.  $\delta^{18}\text{O}$ -depth profiles measured on *G. sacculifer* for all sites used in this study (ODP 848–853). Error bars indicate  $1\sigma$  confidence intervals.

studies have found increased sedimentation rates in EEP cores during glacial periods, but the use of a constant LSR in this study does not significantly affect our results. First, comparison of the oxygen isotopic data with the resulting age models suggests that horizons used for Holocene and glacial averages are appropriate; Holocene horizons (0–10 ka) correspond well with low  $\delta^{18}\text{O}$  and glacial horizons (16–25 ka) correspond well with high  $\delta^{18}\text{O}$ . Second, our MARs and  $^{232}\text{Th}$  fluxes are not significantly affected by age model errors, as noted above (Section 3.2).

It is common for piston cores to incompletely capture core top sediments. For the purposes of this study, we have assigned a zero age to the topmost horizon in each core, as we lack evidence as to the extent of the core top loss. As noted above, the  $\delta^{18}\text{O}$  data for each core indicate that horizons used for Holocene averages are indeed

Holocene in age. The only parameters in this study that are strongly age-model dependent are the focusing factors; estimated age model errors due to possible coretop loss have been included in the reported errors for these values.

### 3.4. Effects of bioturbation

Interpretation of time series data from marine sediments demands an understanding of the effects of bioturbation on the data. Linear sedimentation rates (LSRs) in the present cores range from 0.75 to 3  $\text{cm kyr}^{-1}$ , meaning that latest glacial (16 ka) and earliest Holocene (7 ka) samples used in this study's averages were separated by between 7 and 27 cm. If these samples are mixed, then observed fluxes will underestimate the magnitude and overestimate the duration of deglacial changes.

Relevant data for estimating the effects of bioturbation in our study area come from JGOFS, which included excess  $^{210}\text{Pb}$  and excess  $^{234}\text{Th}$  measurements and observations of benthic fauna along a meridional transect in the equatorial Pacific at  $140^\circ\text{W}$  [42,43]. These researchers report three bioturbation processes affecting near-surface sediments: 1) diffusive mixing of the top 5–10 cm by millimeter-scale macrofauna and meiofauna; 2) homogenization of the top 2–3 cm by burrowing urchins; 3) transport across sediment layers to depths of 3–26 cm by echinurans and other burrowing feeders. Researchers concluded that urchin activity was the dominant mixing process from  $5^\circ\text{S}$  to  $5^\circ\text{N}$ , while low-intensity diffusive mixing was the primary mixing process at  $9^\circ\text{N}$ , where no urchins were observed [43]. Bioturbation intensity was closely tied to particulate organic carbon (POC) flux, as biodiffusive coefficients dropped by over an order of magnitude from the equator to  $9^\circ\text{N}$  [42,43].

As the present study sites have similar organic carbon flux [37] and water depth to those in the JGOFS study, it seems reasonable to assume that bioturbation processes are similar. The relationship between biodiffusive coefficients and POC flux indicates that the greatest bioturbation depth will be at the POC flux maximum near the equator, where there is also the greatest down-core separation between glacial and Holocene samples. Samples at sites 848–851 are taken at 10-cm intervals, well above the mixing depth by urchins, the most dominant mixers, and at the upper limit of diffusive mixing. The least-common mixing process identified by Smith et al. [43], deep transport by burrowers, occasionally mixes to greater depths, but the abrupt changes between 10-cm intervals evidenced at sites 850 and 851 suggest that our sampling interval at the four cores within  $3^\circ$  of the equator is sufficiently wide to avoid significant smoothing by bioturbation.

Due to lower LSRs at sites 852 and 853, samples were taken at 5 and 3 cm intervals, respectively, making these records more susceptible to mixing. Though measured biodiffusive coefficients drop considerably at these distances from the equator [42,43], the nearly linear  $^{232}\text{Th}$  flux record and the low-amplitude  $\delta^{18}\text{O}$  changes at site 853 appear to indicate smoothing by bioturbation. At site 852, where glacial and Holocene samples are separated by 15 cm, the similarity of the flux record to those at sites 848 and 849 and the clear difference from that at site 853 suggests that the LSR is high enough and bioturbation low enough to avoid significant mixing.

### 3.5. $^{232}\text{Th}$ as a proxy for eolian material

Many previous eolian flux studies have chemically separated the operationally defined lithogenic fraction

of sediment samples and referred to this as the eolian component (e.g., [19,8]). This method may not produce consistently accurate results in low-dust areas such as the equatorial Pacific, where MORB-like volcanogenic matter from mid-ocean ridges and ocean island volcanoes has been shown to significantly contaminate the operationally defined lithogenic fraction. A factor analysis of trace element data found that MORB-like volcanogenic material comprises between 44 and 92% of the lithogenic fraction at RC11-210 ( $2^\circ\text{N}$ ,  $140^\circ\text{W}$ ) and between 54 and 78% at DSDP 503B ( $4^\circ\text{N}$ ,  $96^\circ\text{W}$ ) [44]. These results suggest that studies of the operationally defined lithogenic fraction may overestimate eolian fluxes and may report downcore variations that reflect contributions from a variety of sources.

$^{232}\text{Th}$  is likely to be a more accurate proxy for eolian material in many settings. Indeed,  $^{232}\text{Th}$  has been used to track eolian fluxes in several previous studies [45,11,46,27].  $^{232}\text{Th}$  concentrations in continental dust are generally more than an order of magnitude greater than those in MORB-like volcanogenic material (average 10.7 vs. 0.2 ppm) [44,47]. Hence,  $^{232}\text{Th}$  levels in sediments closely track continental inputs and are relatively insensitive to inputs from ocean island and mid-ocean ridge volcanism. Differences in provenance should not greatly affect  $^{232}\text{Th}$ -based estimates of dust flux, as our analysis of dust from source areas around the world suggests that  $^{232}\text{Th}$  concentrations are consistently within 1 ppm of the upper continental crustal average of 10.7 ppm [47] (Fig. 3). One possible exception is dust from Patagonia, which may have Th concentrations of  $\sim 8$  ppm, but this region is unlikely to be a contributor to equatorial Pacific dust fluxes.

In locations where dust fluxes are large and volcanic inputs are relatively minor, we find good agreement between estimates of dust concentrations by the  $^{232}\text{Th}$  and chemical separation methods, and there is no clear advantage to either method. In ODP 658C from Cape Verde, where Saharan dust comprises roughly half of the sediment,  $^{232}\text{Th}$  concentrations and the percentage of non-biogenic sediments correlate remarkably well ( $r^2=0.85$ ) [45]. In our equatorial Pacific setting, where significant MORB-like volcanogenic contamination is likely,  $^{232}\text{Th}$  concentrations are a much better indicator of continental inputs than the operationally defined lithogenic fraction.

While additions of MORB-like volcanic material are not likely to contaminate  $^{232}\text{Th}$  flux data, ash from island and continental arc volcanism is a potential contaminant that must be ruled out. Many ignimbrites and tuffs in the Northern Andes have high Th concentrations (20–30 ppm) [63], suggesting that some Andean ashes may be Th-enriched as well. The close correlation of  $^4\text{He}$  and

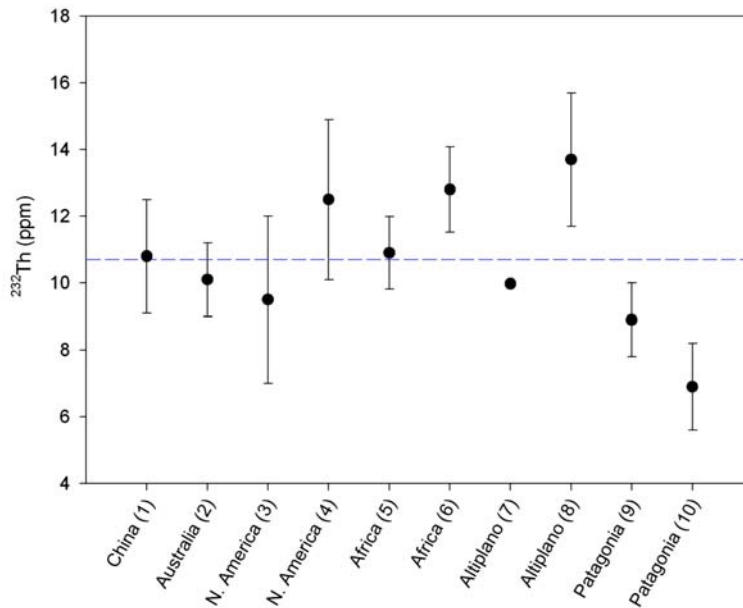


Fig. 3. A compilation of loess and dust data indicating the  $^{232}\text{Th}$  content of various dust source areas. Within error, values fall within 1 ppm of the average Th content of the upper continental crust, shown by the dashed line (10.7 ppm; [47]), with the possible exception of Patagonian dust. Error bars represent one standard deviation of the mean except for (5–7), where error reflects reported variability in Th/Al ratios. Data sources are as follows: (1) Chinese loess ( $n=47$ ) [48–51,44,52,53]; (2) New Zealand loess believed to derive from Australia ( $n=10$ ) [54,55]; (3) North American loess ( $n=4$ ) [55]; (4) airborne dust from the southwest US ( $n=38$ ) [56]; (5) dust collected in the north tropical Atlantic believed to derive from north Africa ( $n=21$ ; assumes [Al]=8.04%) [57]; (6) dust within precipitation in equatorial Africa ( $n=50$ ; assumes [Al]=8.04%) [58]; (7) Altiplano dust ( $n=1$ ) [59]; (8) modern dust in a Bolivian ice core ( $n=640$ ; assumes [Al]=8.04%) [60]; (9) Argentine loess ( $n=7$ ) [61]; (10) Patagonian airborne dust ( $n=13$ ) [62].

$^{232}\text{Th}$  at site 849 argues against significant ash contamination in our records, however (Winckler et al., in prep.).  $^4\text{He}$  in oceanic sediments exists almost exclusively in aged detrital zircons, where it has been produced by U and Th decay [12]. Young volcanic ash has negligible  $^4\text{He}$  concentrations [64,12, F. Marcantonio, unpublished data], so intermittent contamination by continental arc ash would add  $^{232}\text{Th}$  without adding  $^4\text{He}$  and would cause samples to depart significantly from the observed correlation. The correlation between  $^{232}\text{Th}$  and  $^4\text{He}$  is thus most easily explained if both are reflecting an eolian source.

An additional potential contaminant of both operationally defined lithogenic fraction and  $^{232}\text{Th}$  data is hemipelagic continental material, but at more than 1400 km from land our sites are unlikely to receive such inputs [8].

## 4. Results

### 4.1. Mass accumulation rates and focusing factors

$^{230}\text{Th}$ -normalized mass accumulation rates (MARs) were calculated for all samples, and average (0–30 ka), Holocene (0–7 ka), and last glacial (16–25 ka) MARs

were derived for each core (Fig. 4; Table 2). Early Holocene (>7 ka) samples were not included in Holocene averages due to differences between early and late Holocene dust fluxes. By increasing the down-core distance between samples used in Holocene and glacial averages, this approach also minimizes the potential for bioturbation and age model errors to obscure differences between the two time periods. Maximum average MARs ( $\sim 1.0 \text{ g cm}^{-2} \text{ kyr}^{-1}$ ) are found in the four sites within  $3^\circ$  of the equator. MARs for sites 849–851 are not significantly different in any time period ( $1\sigma$ ). MAR values decrease with increasing distance from the equator at the remaining sites to a minimum of  $0.5 \text{ g cm}^{-2} \text{ kyr}^{-1}$  at site 853 ( $7.2^\circ\text{N}$ ), reflecting latitudinal differences in productivity that are consistent with the modern gradient in organic C production [37]. There are no consistent differences between glacial and Holocene MARs within cores, the only significant changes being an increase at site 848 ( $3.0^\circ\text{S}$ ) and a decrease at site 853 ( $7.2^\circ\text{N}$ ) from the last glacial to the Holocene.

Average focusing factors were also calculated for each core (Fig. 4). Errors in focusing factors are larger than for MARs or  $^{232}\text{Th}$  fluxes due to their dependence

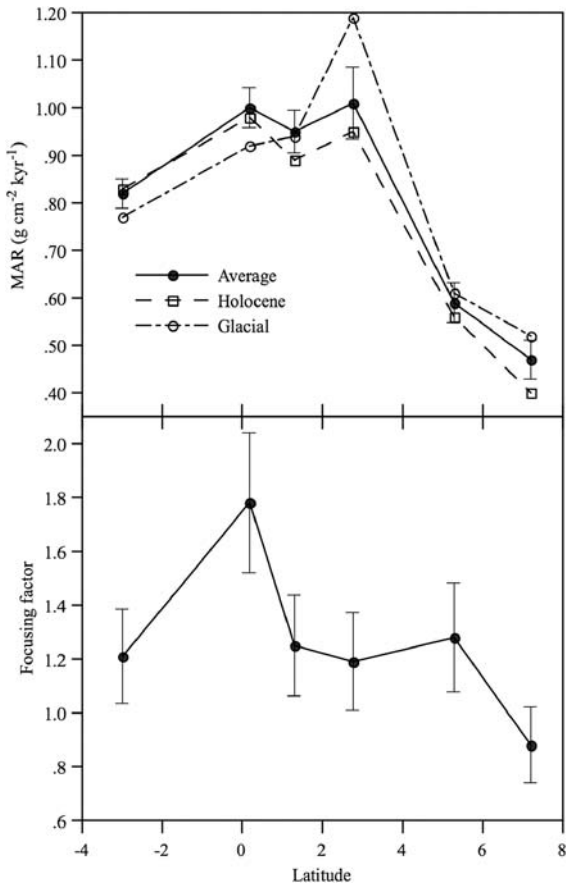


Fig. 4. (Top) Holocene (0–7 ka), last glacial (16–25 ka), and average (0–30 ka) mass accumulation rates (MARs) for all sites, calculated using the  $^{230}\text{Th}$ -profiling method and plotted against latitude. Average MARs do not necessarily lie between glacial and Holocene MARs because the averages include time periods not included in either glacial or Holocene intervals. Error bars on average MARs indicate one standard deviation of the mean. (Bottom) Average focusing factors for all sites plotted against latitude. Values greater than one indicate net focusing.  $1\sigma$  error bars are shown for average values and reflect one standard deviation of mean  $x_s^{230}\text{Th}$  concentrations and age model errors.

on age model and density data. Average focusing factors range from a minimum of 0.9 at site 853 to maximum of 1.8 at site 849, with the remaining four sites all having focusing factors of 1.2–1.3. The focusing factor at site 849 may be overestimated by  $\sim 15\%$  due to local enhancement in  $^{230}\text{Th}$  scavenging.

#### 4.2. $^{232}\text{Th}$ fluxes

Fluxes of  $^{232}\text{Th}$ , our proxy for continental material, were calculated by normalization to  $^{230}\text{Th}$ , as described in Section 3.2. Glacial fluxes of  $^{232}\text{Th}$  are 25–100% higher than Holocene fluxes at all sites except 853, where bioturbation appears to have reduced the am-

plitude of glacial–interglacial differences (Fig. 5). Deglacial changes in the middle of the transect (sites 849–851; 0.2–2.8°N) are almost twice as large as those at the northern and southern ends.

In all time periods,  $^{230}\text{Th}$ -derived fluxes of  $^{232}\text{Th}$  decrease monotonically from the north to the south.  $^{232}\text{Th}$  fluxes in the southernmost core are less than those in the northernmost core by approximately a factor of 2 during the glacial and a factor of 3 during the Holocene. Glacial and Holocene average  $^{232}\text{Th}$  fluxes for each core demonstrate this latitudinal pattern as well as the anomalously large glacial–Holocene flux difference in the middle cores (Fig. 6).

## 5. Discussion

### 5.1. Spatial and temporal patterns in $^{230}\text{Th}$ -normalized MARs and sediment focusing

This study's  $^{230}\text{Th}$ -normalized MAR data bear on the important question of LGM–Holocene changes in productivity in the eastern equatorial Pacific. Recent studies have disagreed as to whether productivity in the region was higher [65] or lower [31] during the last glacial. As all cores are  $>60\%$  carbonate [26], changes in MAR likely reflect changes in calcite supply and preservation. Average  $^{230}\text{Th}$ -normalized MARs do not change significantly along the transect from the last glacial to the Holocene. Because calcite preservation below 3000 m depth is believed to have been higher during the LGM (e.g., [66]), if calcite production were constant or increased in the last glacial we would expect to see an increase in MAR. Our observation of roughly constant MARs is thus consistent with recent findings of decreased calcite production at the LGM in the eastern equatorial Pacific [31].

Calculated focusing factors suggest that most of our sites have been affected by moderate lateral additions of sediment. The degree of focusing indicated (enrichment by factors up to 1.8) is quite consistent with that evident in the seismic surveys associated with ODP Leg 138 and in other surveys in the eastern and central equatorial Pacific, which consistently show enhanced sediment accumulation in depressions and winnowing on slopes [67,33,29].

### 5.2. Spatial and temporal trends in dust flux

$^{232}\text{Th}$  fluxes decrease from 7.2°N to 3.0°S by a factor of  $\sim 2$ –3 throughout the last 30 kyr. Similar cross-equatorial gradients have been observed in all previous studies of equatorial dust flux, including sediment

Table 2  
Oxygen isotope, thorium isotope, and flux data for all samples

ODP core, section, interval (cm)	Depth (mbsf)	Age (ka)	$\delta^{18}\text{O}$ (‰)	$^{232}\text{Th}$ (ng/g)	Blank corr. (%)	$x_s^{230}\text{Th}_o$ (dpm/g)	$^{232}\text{Th}$ flux (dpm m <sup>-2</sup> yr <sup>-1</sup> )	Dust flux (g m <sup>-2</sup> yr <sup>-1</sup> ) <sup>a</sup>	MAR (g cm <sup>-2</sup> kyr <sup>-1</sup> )
138-848B-1H-1,									
0–2	0.00	0	-0.81	174.61	3.1	12.59	0.34	0.13	0.82
10–12	0.10	6	-1.30	164.57	2.9	12.33	0.32	0.12	0.83
20–22	0.20	12	-0.26	189.88	2.7	11.54	0.40	0.15	0.89
30–32	0.30	18	-0.14	258.63	2.0	12.32	0.52	0.20	0.83
40–42	0.40	24	-0.38	351.80	1.5	14.52	0.60	0.23	0.71
50–52	0.50	29	0.18	359.48	1.4	15.08	0.59	0.23	0.68
60–62	0.60	35	-0.21	300.40	1.8	14.56	0.51	0.19	0.71
138-849A-1H-1,									
0–2	0.00	0	-0.87	202.33	2.7	12.61	0.39	0.15	0.81
10–12	0.10	3	-0.83	156.78	3.5	10.51	0.36	0.14	0.97
20–22	0.20	7	-0.75	146.07	3.3	8.87	0.40	0.15	1.16
30–32	0.30	10	-0.48	154.43	3.4	8.13	0.46	0.18	1.26
40–42	0.40	13	-0.26	243.15	2.2	9.82	0.60	0.23	1.04
50–52	0.50	17	0.07	281.20	1.9	10.24	0.67	0.26	1.00
60–62	0.60	20	0.25	375.95	1.4	11.76	0.79	0.30	0.87
70–72	0.70	23	0.01	348.75	1.5	11.38	0.75	0.29	0.90
80–82	0.80	27	-0.10	349.38	1.6	10.53	0.82	0.31	0.97
90–92	0.90	30	-0.41	301.35	1.6	9.99	0.74	0.28	1.03
138-850A-1H-1,									
0–2	0.00	0	-0.64	246.23	2.0	13.62	0.44	0.17	0.74
10–12	0.10	5	-1.36	174.52	3.2	9.68	0.43	0.16	1.04
20–22	0.20	10	-1.22	175.07	3.1	9.50	0.44	0.17	1.06
30–32	0.30	15	-0.46	314.72	1.7	10.54	0.72	0.28	0.96
40–42	0.40	20	-0.20	382.86	1.5	11.62	0.80	0.31	0.87
50–52	0.50	25	-0.39	347.84	1.6	10.09	0.84	0.32	1.00
60–62	0.60	30	-0.59	400.86	1.4	12.09	0.80	0.31	0.84
138-851E-1H-1,									
0–2	0.00	0	-1.30	222.26	2.5	9.34	0.57	0.22	1.08
10–12	0.10	5	-1.27	262.56	2.1	12.29	0.51	0.20	0.82
20–22	0.20	10	-1.29	260.59	1.9	11.20	0.56	0.21	0.90
30–32	0.30	15	-0.63	409.13	1.3	11.03	0.90	0.34	0.91
40–42	0.40	20	-0.36	388.95	1.2	10.12	0.93	0.36	0.99
50–52	0.50	25	-0.47	275.90	1.8	7.27	0.91	0.35	1.38
60–62	0.60	30	-0.55	355.44	1.6	9.24	0.93	0.36	1.09
138-852A-1H-1,									
0–2	0.00	0	-1.44	593.64	1.0	15.60	0.95	0.36	0.66
5–7	0.05	4	-1.05	808.80	0.7	22.18	0.91	0.35	0.46
10–12	0.10	8	-1.29	602.70	0.8	14.69	1.02	0.39	0.70
15–17	0.15	12	-0.85	956.68	0.5	20.09	1.19	0.46	0.51
20–22	0.20	16	-0.74	1021.83	0.5	20.98	1.22	0.47	0.49
25–27	0.25	20	-0.34	868.89	0.6	19.03	1.14	0.44	0.54
30–35	0.30	24	-0.57	593.14	0.9	13.10	1.13	0.43	0.79
35–37	0.35	28	-0.65	558.05	1.0	12.96	1.07	0.41	0.80
40–42	0.40	32	-0.58	627.78	0.8	14.96	1.04	0.40	0.69
138-853B-1H-1,									
0–2	0.00	0	-1.10	1177.11	0.5	25.04	1.13	0.43	0.40
3–5	0.03	4	-1.10	1236.90	0.4	24.13	1.23	0.47	0.41
6–8	0.06	8	-0.88	1389.62	0.4	25.98	1.29	0.49	0.38
9–11	0.09	12	ND	1010.58	0.5	18.95	1.28	0.49	0.52
12–14	0.12	16	-0.61	1460.87	0.4	26.45	1.33	0.51	0.37
15–17	0.15	20	-0.55	1045.01	0.5	18.73	1.34	0.51	0.53

Table 2 (continued)

ODP core, section, interval (cm)	Depth (mbsf)	Age (ka)	$\delta^{18}\text{O}$ (‰)	$^{232}\text{Th}$ (ng/g)	Blank corr. (%)	$x_s^{230}\text{Th}_o$ (dpm/g)	$^{232}\text{Th}$ flux ( $\text{dpm m}^{-2} \text{ yr}^{-1}$ )	Dust flux ( $\text{g m}^{-2} \text{ yr}^{-1}$ ) <sup>a</sup>	MAR ( $\text{g cm}^{-2} \text{ kyr}^{-1}$ )
138-853B-1H-1									
18–20	0.18	24	−0.87	891.86	0.6	14.83	1.44	0.55	0.67

<sup>a</sup> Calculated assuming a Th concentration of 10.7 ppm ([47]; see Section 3.5).

[11,8], sediment trap [68], satellite [69,18] and modeling [17,70–72] studies, though this study provides the highest-resolution results to date.

The meridional gradient in dust flux observed at 110°W appears to be a robust feature reflecting the boundary between high North Pacific and low South Pacific dust levels. Dust deposition in the equatorial Pacific is dominated by precipitation scavenging [73]. Studies of northern-sourced pollutants find very steep gradients across the ITCZ [74], indicating that inter-hemispheric transport of aerosols is greatly limited by high precipitation levels and deep convection in the ITCZ. It therefore seems reasonable that dust provenance should change across the ITCZ as well; still, very little is known about the provenance of dust at our sites. Researchers studying ocean sediments in the central and eastern equatorial Pacific have tended to emphasize the importance of Chinese and North and South American dust sources [8,75], while models based on satellite data tend to suggest Africa and Australia as additional important sources [76]. On a general level, existing Nd and Pb isotope [20,21] and clay mineralogy data [77,78], as well as dust models [76], suggest a change from northern-sourced to southern-sourced dust between 5°N and 0°N in the equatorial Pacific. We provisionally accept these basic findings, which suggest that our transect provides a record of dust production and deposition in both hemispheres, while acknowledging the need for more detailed provenance studies.

Increased glacial  $^{232}\text{Th}$  fluxes in all cores are consistent with elevated atmospheric dust levels in both hemispheres of the Pacific Ocean during the most recent glacial period. This finding agrees with previous studies of glacial dustiness in both hemispheres (e.g., [7,8]), recent studies of equatorial Pacific dust flux [11,12], and model results [79,71,72]. Anderson et al. [11] measured  $^{230}\text{Th}$ -normalized  $^{232}\text{Th}$  fluxes in a similar transect at 140°W (Fig. 7). The meridional pattern of dust deposition is quite similar to that in this study, as  $^{232}\text{Th}$  accumulation rates decrease by approximately a factor of 3 from 4°N to 5°S along 140°W. Glacial–Holocene differences are also similar to those in this study. Sedimentation rates at 140°W sites are lower ( $\sim .5$  to  $1.6 \text{ cm kyr}^{-1}$ ) than at the present study sites ( $.75$  to  $3 \text{ cm kyr}^{-1}$ ), and so bioturbation may play a significant

role in reducing LGM–Holocene differences in cores at the northern and southern ends of the 140°W transect [11]. Together, the results from these two studies provide a compelling indication that dust fluxes are consistent in magnitude and climate dependence throughout the central and eastern equatorial Pacific.

Our data may not be consistent with findings in another EEP core, DSDP 503B (4°N, 96°W), indicating reduced glacial dust fluxes [8]. These results have been interpreted as suggesting reduced dust production in tropical and subtropical South America [8]. Though the present study includes only one glacial–interglacial transition, the consistency of the records in our six cores showing higher fluxes in the last glacial than in the Holocene leads us to question whether the EEP has indeed been dustier during interglacial periods, as the data from 503B suggest. It may be that these two study sites, separated by 15° of longitude, reflect different dust sources. Alternatively, the operationally defined lithogenic fraction data at 503B may suffer from significant and time-varying contamination by volcanogenic matter ( $\sim 50$ – $80\%$ ; [44]). An additional potential source of error is the age model used for flux calculations at 503B, which is based on benthic  $\delta^{18}\text{O}$  data with a resolution of 1 sample per  $\sim 15$  kyr, making accurate correlation to SPECMAP difficult. To the extent that EEP dust derives from South America, our data are consistent with syntheses of lake and pollen [80] and ice core [10] data showing that while high elevations in central South America were wetter during the glacial, conditions throughout northern South America were drier and dustier.

Our data suggest that dust levels fell earliest at the southern end of the transect, beginning around 20 ka, and that high glacial dust levels persisted until approximately 15 ka at the northern sites (Fig. 5). It will be interesting to see if these results are corroborated by studies with better age controls.

### 5.3. Deglacial changes in ITCZ dynamics

Past studies have used changes in dust flux, mineralogy and grain size to track the position of the Pacific ITCZ on time scales of  $> 100$  kyr [19,23,24]. In this study

we make the first attempt to use dust fluxes to identify changes in the Pacific ITCZ during the last deglaciation. We begin by investigating the difference in the meridional dust flux gradient between the Holocene and the last

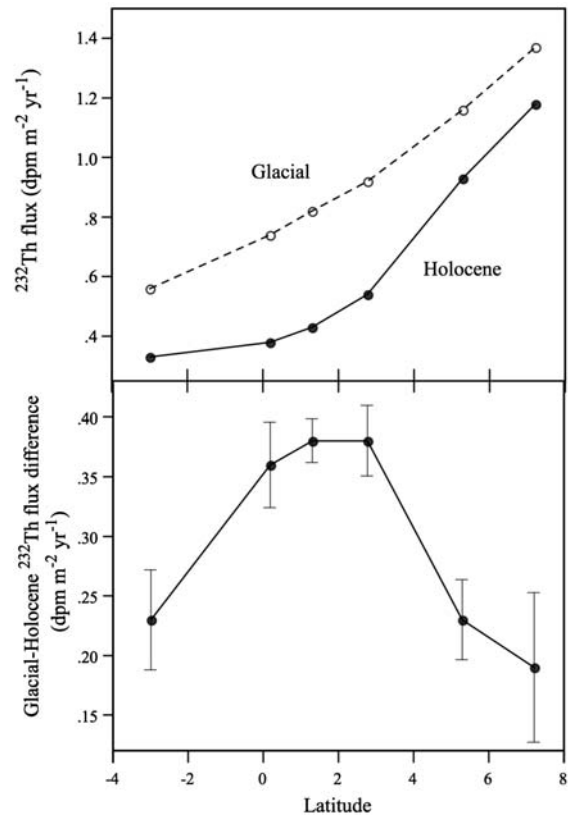
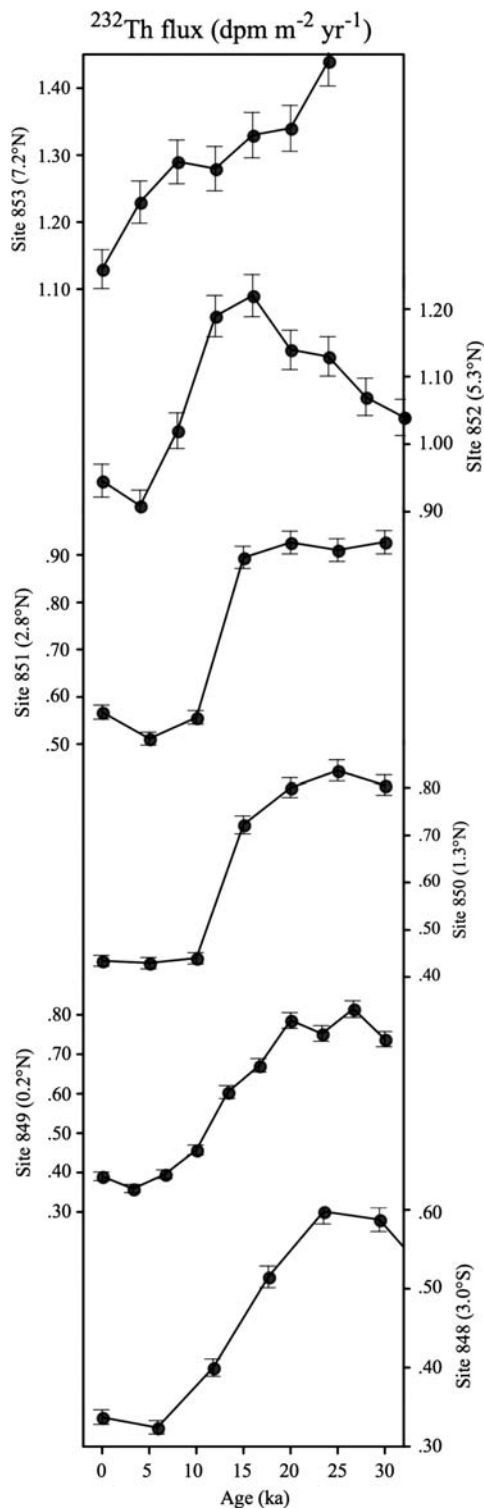


Fig. 6. (Top) Holocene and last glacial average  $^{230}\text{Th}$ -normalized  $^{232}\text{Th}$  fluxes for each site, plotted against latitude. Error bars reflect one standard deviation of the mean. Both time periods show  $^{232}\text{Th}$  flux decreasing towards the south, though the meridional gradient is reduced during the last glacial. (Bottom) Differences between glacial and Holocene  $^{232}\text{Th}$  flux values for each site plotted against latitude, showing maximum deglacial changes between 0.2 and 2.8 °N.  $1\sigma$  error bars are shown.

glacial. Our results indicate a steeply curving flux gradient during the Holocene and a much shallower, nearly linear gradient during the last glacial (Fig. 6). In the Holocene, it appears that the ITCZ efficiently scavenges northern hemisphere dust, as nearly 50% of the drop in dust flux between 7.2°N and 3.0°S occurs just south of the modern range of the ITCZ, between 5.3 and 2.8°N, and dust fluxes at sites south of 3°N are only slightly higher than at 3°S. During the last glacial, the drop in dust flux between 5.3 and 2.8°N is less than 30% of the total north–south difference, and dust flux diminishes in

Fig. 5. Time series of  $^{230}\text{Th}$ -normalized  $^{232}\text{Th}$  accumulation rates for each site. Error bars indicate  $1\sigma$  confidence intervals based on reproducibility of  $^{230}\text{Th}$  and  $^{232}\text{Th}$  values and estimated error in  $^{232}\text{Th}$  blank corrections. With the exception of the record from site 853, which has been smoothed by bioturbation, sites show a consistent pattern of decreasing  $^{232}\text{Th}$  flux from approximately 20 ka to 5 ka.

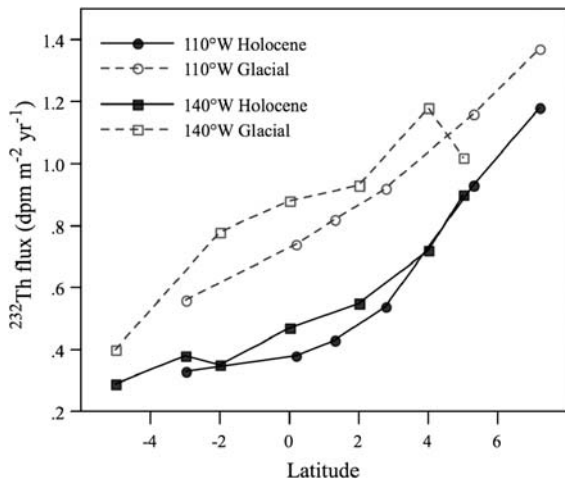


Fig. 7. Holocene and last glacial average  $^{232}\text{Th}$  fluxes along meridional transects at  $110^\circ\text{W}$  (this study) and  $140^\circ\text{W}$  [11]. The two records are quite consistent, with fluxes slightly higher at  $110^\circ\text{W}$  in both the last glacial and the Holocene. Glacial–Holocene differences at the northern and southern ends of the  $140^\circ\text{W}$  transect are believed to be reduced due to bioturbation [11]. Holocene averages are from all samples between 0 and 7 ka, with the exception of cores at  $4^\circ\text{N}$  and  $5^\circ\text{N}$  along  $140^\circ\text{W}$ , for which the first available value after 7 ka was used. Glacial averages include all samples between 16 and 25 ka.

a nearly linear fashion along the transect. As a result of this change in gradient, fluxes at sites in the middle of the transect ( $849\text{--}851$ ;  $0.2\text{--}2.8^\circ\text{N}$ ) are much closer to northern core values in the glacial than in the Holocene, and these sites experience deglacial dust flux changes nearly twice as large as those at the northern and southern ends of the transect (Fig. 6).

We suggest that these changes may reflect less efficient dust scavenging in the EEP ITCZ during the last glacial due to reduced convective intensity and precipitation, both of which have been inferred from proxy studies [16] and suggested by models [3]. Decreased scavenging efficiency would allow more inter-hemispheric dust transport, smoothing the meridional dust flux gradient as observed. An alternative explanation is that the latitude of ITCZ scavenging was more variable in the last glacial period producing a smoother meridional gradient. This increased variability could have been anywhere from seasonal to millennial in scale.

Previous studies have provided evidence for a southerly displacement of the ITCZ's mean latitude over the western Atlantic, South America, and the EEP during the LGM (e.g., [14,15]). Our results are not inconsistent with these findings, but we do not believe that the present results require a southerly mean ITCZ position at the LGM. While a southerly displacement of the mean ITCZ with no change in scavenging efficiency would produce a similar pattern of deglacial flux

changes (maximum changes just south of the modern range of the ITCZ), it would not by itself produce a smoother glacial flux gradient.

We do not believe that the observed changes in the dust flux gradient can be explained solely by increased transport of dust to the area during the last glacial, without any changes in the ITCZ. Atmospheric dust levels several times higher than those in the glacial equatorial Pacific are present in the northern tropical Atlantic today, but a steep dust flux gradient exists [70,69,18,76]. We therefore interpret increases in relative dust deposition in the middle of the transect as representing a change in scavenging efficiency and/or latitudinal variability rather than a change in dust supply.

## 6. Conclusions

This study presents one of the most complete temporal and spatial surveys to date of eolian dust flux to the equatorial ocean over the past 30 kyr. We use  $^{232}\text{Th}$  as a proxy for eolian input and normalize to  $x_s^{230}\text{Th}_0$  to calculate fluxes that are independent of our age model and that account for sediment focusing. Our findings indicate that dust fluxes in both hemispheres of the eastern equatorial Pacific were 25–100% higher during the last glacial, consistent with recent findings in the central equatorial Pacific [11].

Throughout the past 30 kyr, dust fluxes along  $110^\circ\text{W}$  have decreased from  $7^\circ\text{N}$  to  $3^\circ\text{S}$  by a factor of 2 to 3, reflecting scavenging of high northern hemisphere atmospheric dust levels by precipitation at the ITCZ. A smoothing of the slope of the meridional dust flux gradient during the last glacial may be explained by less efficient dust scavenging at this time, most likely due to reduced convection and precipitation by the glacial ITCZ, or by increased variability in the ITCZ location. Our results do not require a southern displacement of the glacial ITCZ, though they also do not contradict previous results indicating LGM–Holocene ITCZ movement. More detailed provenance studies may assist in determining the relative importance of changes in ITCZ convective intensity and position in producing the observed glacial–interglacial flux differences. This first attempt at using dust fluxes to track the Pacific ITCZ over the last deglaciation suggests that similar transects may be useful in characterizing past ITCZ conditions in other regions and over longer time periods.

## Acknowledgments

We would like to thank Ali Pourmand for his generous technical assistance and the core curators at the Ocean

Drilling Program for providing samples. Thanks are also due to Jess Adkins, Robert Anderson, and Mark Siddall for providing data. This paper was improved by constructive comments by Robert Anderson, Martin Frank, Gisela Winckler, David Rea, Mark Siddall, and anonymous reviewers. This research used samples provided by the Ocean Drilling Program (ODP). ODP is sponsored by the U.S. National Science Foundation (NSF) and participating countries under management of Joint Oceanographic Institutions (JOI), Inc. This work was supported by NSF grant OCE-0402311 and the NSF Graduate Research Fellowship Program.

## References

- [1] N.M. Mahowald, M. Yoshioka, W.D. Collins, A.J. Conley, D.W. Fillmore, D.B. Coleman, Climate response and radiative forcing from mineral aerosols during the last glacial maximum, pre-industrial, current and double-carbon dioxide climates, *Geophys. Res. Lett.* 33 (2006) L20705, doi:10.1029/2006GL026126.
- [2] R.L. Miller, I. Tegen, Climate response to soil dust aerosols, *J. Climate* 11 (1998) 3247–3267.
- [3] R.L. Miller, I. Tegen, J. Perlwitz, Surface radiative forcing by soil dust aerosols and the hydrologic cycle, *J. Geophys. Res. - Atmos.* 109 (2004) D04203, doi:10.1029/2003JD004085.
- [4] T.S. Ivanochko, R.S. Ganeshram, G.J.A. Brummer, G. Ganssen, S.J.A. Jung, S.G. Moreton, D. Kroon, Variations in tropical convection as an amplifier of global climate change at the millennial scale, *Earth Planet. Sci. Lett.* 235 (2005) 302–314.
- [5] L. Bopp, K.E. Kohfeld, C. Le Quere, O. Aumont, Dust impact on marine biota and atmospheric CO<sub>2</sub> during glacial periods, *Paleoceanography* 18 (2003) A1046, doi:10.1029/2002PA000810.
- [6] K.H. Coale, K.S. Johnson, S.E. Fitzwater, R.M. Gordon, S. Tanner, F.P. Chavez, L. Ferioli, C. Sakamoto, P. Rogers, F. Millero, P. Steinberg, P. Nightingale, D. Cooper, W.P. Cochlan, M.R. Landry, J. Constantinou, G. Rollwagen, A. Trasvina, R. Kudela, A massive phytoplankton bloom induced by an ecosystem-scale iron fertilization experiment in the equatorial Pacific Ocean, *Nature* 383 (1996) 495–501.
- [7] K.E. Kohfeld, S.P. Harrison, DIRTMAP: the geological record of dust, *Earth-Sci. Rev.* 54 (2001) 81–114.
- [8] D.K. Rea, The paleoclimatic record provided by eolian deposition in the Deep-Sea — the geologic history of wind, *Rev. Geophys.* 32 (1994) 159–195.
- [9] W.F. Ruddiman, Tropical Atlantic terrigenous fluxes since 25,000 yrs BP, *Mar. Geol.* 136 (1997) 189–207.
- [10] L.G. Thompson, E. Mosley-Thompson, K.A. Henderson, Ice-core palaeoclimate records in tropical South America since the Last Glacial Maximum, *J. Quat. Sci.* 15 (2000) 377–394.
- [11] R.F. Anderson, M.Q. Fleisher, Y. Lao, Glacial–interglacial variability in the delivery of dust to the central equatorial Pacific Ocean, *Earth Planet. Sci. Lett.* 242 (2006) 406–414.
- [12] D.B. Patterson, K.A. Farley, M.D. Norman, He-4 as a tracer of continental dust: a 1.9 million year record of aeolian flux to the west equatorial Pacific Ocean, *Geochim. Cosmochim. Acta* 63 (1999) 615–625.
- [13] K.E. Trenberth, G.W. Branstator, D. Karoly, A. Kumar, N.C. Lau, C. Ropelewski, Progress during TOGA in understanding and modeling global teleconnections associated with tropical sea surface temperatures, *J. Geophys. Res. -Oceans* 103 (1998) 14291–14324.
- [14] A. Koutavas, J. Lynch-Stieglitz, Variability of the marine ITCZ over the eastern Pacific during the past 30,000 years: regional perspective and global context, in: R.S. Bradley, H.F. Diaz (Eds.), *The Hadley Circulation: Present, Past and Future*, Kluwer Academic Publishers, 2004, pp. 347–369.
- [15] L.C. Peterson, G.H. Haug, K.A. Hughen, U. Rohl, Rapid changes in the hydrologic cycle of the tropical Atlantic during the last glacial, *Science* 290 (2000) 1947–1951.
- [16] A. Koutavas, J. Lynch-Stieglitz, Glacial–interglacial dynamics of the eastern equatorial Pacific cold tongue Intertropical Convergence Zone system reconstructed from oxygen isotope records, *Paleoceanography* 18 (2003) 1089, doi:10.1029/2003PA000894.
- [17] R.A. Duce, The atmospheric input of trace species to the world ocean, *Glob. Biogeochem. Cycles* 5 (1991) 193–259.
- [18] R.B. Husar, J.M. Prospero, L.L. Stowe, Characterization of tropospheric aerosols over the oceans with the NOAA advanced very high resolution radiometer optical thickness operational product, *J. Geophys. Res. - Atmos.* 102 (1997) 16889–16909.
- [19] S.A. Hovan, Late Cenozoic atmospheric circulation intensity and climatic history recorded by eolian deposition in the eastern equatorial Pacific Ocean, Leg 138, in: N.G. Pisias, L.A. Mayer, T.R. Janecek, A. Palmer-Julson, T.H. van Andel (Eds.), *Proceedings of the Ocean Drilling Program, Scientific Results*. Ocean Drilling Program, College Station, Texas, 1995, pp. 615–625.
- [20] C.E. Jones, A.N. Halliday, D.K. Rea, R.M. Owen, Neodymium isotopic variations in North Pacific modern silicate sediment and the insignificance of detrital REE contributions to seawater, *Earth Planet. Sci. Lett.* 127 (1994) 55–66.
- [21] C.E. Jones, A.N. Halliday, D.K. Rea, R.M. Owen, Eolian inputs of lead to the North Pacific, *Geochim. Cosmochim. Acta* 64 (2000) 1405–1416.
- [22] S. Nakai, A.N. Halliday, D.K. Rea, Provenance of Dust in the Pacific–Ocean, *Earth Planet. Sci. Lett.* 119 (1993) 143–157.
- [23] K. Hyeong, S.H. Park, C.M. Yoo, K.H. Kim, Mineralogical and geochemical compositions of the eolian dust from the northeast equatorial Pacific and their implications on paleolocation of the Intertropical Convergence Zone, *Paleoceanography* 20 (2005) A1010, doi:10.1029/2004PA00153.
- [24] M. Lyle, et al., Leg 199 Summary, *Proc. Ocean Drill. Program, Initial Rep.* (2002) 1–87.
- [25] P. Xie, P.A. Arkin, Global Precipitation: a 17-year monthly analysis based on gauge observations, satellite estimates, and numerical model outputs, *Bull. Am. Meteorol. Soc.* 78 (1997) 2539–2558.
- [26] L.A. Mayer, N.G. Pisias, T.R. Janecek, et al., *Proceedings of the Ocean Drilling Program, Initial Reports*, Ocean Drilling Program, College Station, Texas, 1992.
- [27] A. Pourmand, F. Marcantonio, H. Schulz, Variations in productivity and eolian fluxes in the northeastern Arabian Sea during the past 110 ka, *Earth Planet. Sci. Lett.* 221 (2004) 39–54.
- [28] R. Francois, M. Frank, M.M.R. van der Loeff, M.P. Bacon, Th-230 normalization: an essential tool for interpreting sedimentary fluxes during the late Quaternary, *Paleoceanography* 19 (2004), doi:10.1029/2003PA000994.
- [29] N.C. Mitchell, M.W. Lyle, Patchy deposits of Cenozoic pelagic sediments in the central Pacific, *Geology* 33 (2005) 49–52.
- [30] S.S., Kienast, M., Kienast, A.C., Mix, S.E., Calvert, R., Francois, Thorium-230 normalized particle flux and sediment focusing in the Panama Basin region during the last 30,000 years, *Paleoceanography* in press, doi:10.1029/2006PA001357.

- [31] P. Loubere, F. Mekik, R. Francois, S. Pichat, Export fluxes of calcite in the eastern equatorial Pacific from the Last Glacial Maximum to present, *Paleoceanography* 19 (2004) A2018, doi:10.1029/2003PA000986.
- [32] R. Francois, M. Frank, M. Rutgers van der Loeff, M.P. Bacon, W. Geibert, S. Kienast, R.F. Anderson, L. Bradtmiller, Z. Chase, G. Henderson, F. Marcantonio, S.E. Allen, Comment on “Do geochemical estimates of sediment focusing pass the sediment test in the equatorial Pacific?” by M. Lyle et al., *Paleoceanography* 22 (in press) PA1216, doi:10.1029/2005PA001235.
- [33] M. Lyle, N. Mitchell, N. Pisias, A. Mix, J.I. Martinez, A. Paytan, Do geochemical estimates of sediment focusing pass the sediment test in the equatorial Pacific? *Paleoceanography* 20 (2005) A1005, doi:10.1029/2004PA001019.
- [34] J.C. Scholten, J. Fietzke, A. Mangini, P. Stoffers, T. Rixen, B. Gaye-Haake, T. Blanz, V. Ramaswamy, F. Sirocko, H. Schulz, V. Ittekkot, Radionuclide fluxes in the Arabian Sea: the role of particle composition, *Earth Planet. Sci. Lett.* 230 (2005) 319–337.
- [35] E.F. Yu, R. Francois, M.P. Bacon, A.P. Fleer, Fluxes of Th-230 and Pa-231 to the deep sea: implications for the interpretation of excess Th-230 and Pa-231/Th-230 profiles in sediments, *Earth Planet. Sci. Lett.* 191 (2001) 219–230.
- [36] G.M. Henderson, C. Heinze, R.F. Anderson, A.M.E. Winguth, Global distribution of the Th-230 flux to ocean sediments constrained by GCM modelling, *Deep-Sea Res., Part 1, Oceanogr. Res. Pap.* 46 (1999) 1861–1893.
- [37] D. Antoine, J.M. Andre, A. Morel, Oceanic primary production. 2. Estimation at global scale from satellite (coastal zone color scanner) chlorophyll, *Glob. Biogeochem. Cycles* 10 (1996) 57–69.
- [38] S.M. Higgins, R.F. Anderson, F. Marcantonio, P. Schlosser, M. Stute, Sediment focusing creates 100-ka cycles in interplanetary dust accumulation on the Ontong Java Plateau, *Earth Planet. Sci. Lett.* 203 (2002) 383–397.
- [39] F. Marcantonio, R.F. Anderson, S. Higgins, M. Stute, P. Schlosser, P. Kubik, Sediment focusing in the central equatorial Pacific Ocean, *Paleoceanography* 16 (2001) 260–267.
- [40] S. Mukhopadhyay, K.A. Farley, New insights into the carrier phase(s) of extraterrestrial <sup>3</sup>He in geologically old sediments, *Geochim. Cosmochim. Acta* 70 (2006) 5061–5073.
- [41] N.J. Shackleton, S. Crowhurst, T. Hagelberg, N.G. Pisias, D.A. Schneider, A new late Neogene time scale: application to Leg 138 sites, in: N.G. Pisias, L.A. Mayer, T.R. Janecek, A. Palmer-Julson, T.H. van Andel (Eds.), *Proceedings of the Ocean Drilling Program, Scientific Results*, 1995, pp. 73–98.
- [42] R.H. Pope, D.J. Demaster, C.R. Smith, H. Seltmann, Rapid bioturbation in equatorial Pacific sediments: evidence from excess Th-234 measurements, *Deep-Sea Res., Part 2, Top. Stud. Oceanogr.* 43 (1996) 1339–1364.
- [43] C.R. Smith, W. Berelson, D.J. Demaster, F.C. Dobbs, D. Hammond, D.J. Hoover, R.H. Pope, M. Stephens, Latitudinal variations in benthic processes in the abyssal equatorial Pacific: control by biogenic particle flux, *Deep-Sea Res., Part 2, Top. Stud. Oceanogr.* 44 (1997) 2295–2317.
- [44] A.M. Olivarez, R.M. Owen, D.K. Rea, Geochemistry of eolian dust in pacific pelagic sediments — implications for paleoclimatic interpretations, *Geochim. Cosmochim. Acta* 55 (1991) 2147–2158.
- [45] J. Adkins, P. deMenocal, G. Eshel, The “African humid period” and the record of marine upwelling from excess <sup>230</sup>Th in Ocean Drilling Program Hole 658C, *Paleoceanography* 21 (2006) A4203, doi:10.1029/2005PA001200.
- [46] F. Marcantonio, R.F. Anderson, S. Higgins, M.Q. Fleisher, M. Stute, P. Schlosser, Abrupt intensification of the SW Indian Ocean monsoon during the last deglaciation: constraints from Th, Pa, and He isotopes, *Earth Planet. Sci. Lett.* 184 (2001) 505–514.
- [47] S.R. Taylor, S.M. McLennan, *The Continental Crust: Its Composition and Evolution*, Blackwell Scientific, Oxford, 1985.
- [48] Z.L. Ding, J.M. Sun, S.L. Yang, T.S. Liu, Geochemistry of the Pliocene red clay formation in the Chinese Loess Plateau and implications for its origin, source provenance and paleoclimate change, *Geochim. Cosmochim. Acta* 65 (2001) 901–913.
- [49] S. Gallet, B.M. Jahn, M. Torii, Geochemical characterization of the Luochuan loess-paleosol sequence, China, and paleoclimatic implications, *Chem. Geol.* 133 (1996) 67–88.
- [50] B.M. Jahn, S. Gallet, J.M. Han, Geochemistry of the Xining, Xifeng and Jixian sections, Loess Plateau of China: eolian dust provenance and paleosol evolution during the last 140 ka, *Chem. Geol.* 178 (2001) 71–94.
- [51] C.Q. Liu, A. Masuda, A. Okada, S. Yabuki, J. Zhang, Z.L. Fan, A geochemical study of loess and desert sand in northern China — implications for continental-crust weathering and composition, *Chem. Geol.* 106 (1993) 359–374.
- [52] E.T. Weber, R.M. Owen, G.R. Dickens, A.N. Halliday, C.E. Jones, D.K. Rea, Quantitative resolution of eolian continental crustal material and volcanic detritus in North Pacific surface sediment, *Paleoceanography* 11 (1996) 115–127.
- [53] E.T. Weber, R.M. Owen, G.R. Dickens, D.K. Rea, Causes and implications of the middle rare earth element depletion in the eolian component of North Pacific sediment, *Geochim. Cosmochim. Acta* 62 (1998) 1735–1744.
- [54] S.K. Marx, B.S. Kamber, H.A. McGowan, Provenance of long-travelled dust determined with ultra-trace-element composition: a pilot study with samples from New Zealand glaciers, *Earth Surf. Processes Landf.* 30 (2005) 699–716.
- [55] S.R. Taylor, S.M. McLennan, M.T. McCulloch, Geochemistry of loess, continental crustal composition and crustal model ages, *Geochim. Cosmochim. Acta* 47 (1983) 1897–1905.
- [56] M.C. Reheis, J.R. Budahn, P.J. Lamothe, Elemental analyses of modern dust in southern Nevada and California, USGS Open-File Report 99-0531 (1999) web release.
- [57] A.M. Johansen, R.L. Siefert, M.R. Hoffmann, Chemical composition of aerosols collected over the tropical North Atlantic Ocean, *J. Geophys. Res. - Atmos.* 105 (2000) 15277–15312.
- [58] R. Freydier, B. Dupre, J.P. Lacaux, Precipitation chemistry in intertropical Africa, *Atmos. Environ.* 32 (1998) 749–765.
- [59] C. Placzek, P.J. Patchett, J. Quade, J.D.M. Wagner, Strategies for successful U–Th dating of paleolake carbonates: an example from the Bolivian Altiplano, *Geochim. Geophys. Geosyst.* 7 (2006) Q05024, doi:10.1029/2005GC001157.
- [60] A. Correia, R. Freydier, R.J. Delmas, J.C. Simoes, J.D. Taupin, B. Dupre, P. Artaxo, Trace elements in South America aerosol during 20th century inferred from a Nevado Illimani ice core, Eastern Bolivian Andes (6350 m asl), *Atmos. Chem. Phys.* 3 (2003) 1337–1352.
- [61] S. Gallet, B.-m. Jahn, B. Van Vliet Lanoe, A. Dia, E. Rossello, Loess geochemistry and its implications for particle origin and composition of the upper continental crust, *Earth Planet. Sci. Lett.* 156 (1998) 157–172.
- [62] D.M. Gaiero, P.J. Depetris, J.L. Probst, S.M. Bidart, L. Leleyter, The signature of river- and wind-borne materials exported from Patagonia to the southern latitudes: a view from REEs and implications for paleoclimatic interpretations, *Earth Planet. Sci. Lett.* 219 (2004) 357–376.
- [63] P.P. Lehti, J.C. Thouret, G. Womer, M. Fornari, Neogene and Quaternary ignimbrites in the area of Arequipa, Southern Peru:

- stratigraphical and petrological correlations, *J. Volcanol. Geotherm. Res.* 154 (2006) 251–275.
- [64] F. Marcantonio, K.K. Turekian, S. Higgins, R.F. Anderson, M. Stute, P. Schlosser, The accretion rate of extraterrestrial He-3 based on oceanic Th-230 flux and the relation to Os isotope variation over the past 200,000 years in an Indian Ocean core, *Earth Planet. Sci. Lett.* 170 (1999) 157–168.
- [65] M. Lyle, A. Mix, N. Pisias, Patterns of CaCO<sub>3</sub> deposition in the eastern tropical Pacific Ocean for the last 150 kyr: evidence for a southeast Pacific depositional spike during marine isotope stage (MIS) 2, *Paleoceanography* 17 (2002) A1013, doi:10.1029/2000PA000538.
- [66] J.W. Farrell, W.L. Prell, Climatic change and CaCO<sub>3</sub> preservation: an 800000 year bathymetric reconstruction from the central equatorial Pacific Ocean, *Paleoceanography* 4 (1989) 447–466.
- [67] S.F. Bloomer, L.A. Mayer, J.T.C. Moore, T.C., Seismic stratigraphy of the Eastern Equatorial Pacific Ocean: paleoceanographic implications, in: N.G. Pisias, L.A. Mayer, T.R. Janecek, A. Palmer-Julson, T.H. van Andel (Eds.), *Proceedings of the Ocean Drilling Program, Scientific Results. Ocean Drilling Program, College Station, Texas, 1995*, pp. 537–553.
- [68] S. Honjo, J. Dymond, R. Collier, S.J. Manganini, Export production of particles to the interior of the equatorial Pacific-Ocean during the 1992 Eqpac experiment, *Deep-Sea Res., Part 2, Top. Stud. Oceanogr.* 42 (1995) 831–870.
- [69] J.R. Herman, P.K. Bhartia, O. Torres, C. Hsu, C. Seftor, E. Celarier, Global distribution of UV-absorbing aerosols from Nimbus 7/TOMS data, *J. Geophys. Res.* 102 (1997) 16,911–16,922.
- [70] P. Ginoux, M. Chin, I. Tegen, J.M. Prospero, B. Holben, O. Dubovik, S.J. Lin, Sources and distributions of dust aerosols simulated with the GOCART model, *J. Geophys. Res. - Atmos.* 106 (2001) 20255–20273.
- [71] N.M. Mahowald, D.R. Muhs, S. Levis, P.J. Rasch, M. Yoshioka, C.S. Zender, C. Luo, Change in atmospheric mineral aerosols in response to climate: las glacial period, preindustrial, modern, and doubled carbon dioxide climates, *J. Geophys. Res. - Atmos.* 111 (in press) D10202, doi:10.1029/12005JD006653.
- [72] M. Werner, I. Tegen, S.P. Harrison, K.E. Kohfeld, I.C. Prentice, Y. Balkanski, H. Rodhe, C. Roelandt, Seasonal and interannual variability of the mineral dust cycle under present and glacial climate conditions, *J. Geophys. Res. - Atmos.* 107 (2002) 4744, doi:10.1029/2002JD002365.
- [73] C.S. Zender, H.S. Bian, D. Newman, Mineral Dust Entrainment and Deposition (DEAD) model: description and 1990s dust climatology, *J. Geophys. Res. - Atmos.* 108 (2003) 4416, doi:10.1029/2002JD002775.
- [74] G.L. Gregory, D.J. Westberg, M.C. Shipham, D.R. Blake, R.E. Newell, H.E. Fuelberg, R.W. Talbot, B.G. Heikes, E.L. Atlas, G.W. Sachse, B.A. Anderson, D.C. Thornton, Chemical characteristics of Pacific tropospheric air in the region of the Intertropical Convergence Zone and South Pacific Convergence Zone, *J. Geophys. Res. - Atmos.* 104 (1999) 5677–5696.
- [75] A.M. Stancin, J.D. Gleason, D.K. Rea, R.M. Owen, J. Moore, T.C. Blum, J.D. Hovan, Radiogenic isotopic mapping of late Cenozoic eolian and hemipelagic sediment distribution in the east-central Pacific, *Earth Planet. Sci. Lett.* 248 (2006) 840–850.
- [76] C. Luo, N.M. Mahowald, J. del Corral, Sensitivity study of meteorological parameters on mineral aerosol mobilization, transport, and distribution, *J. Geophys. Res. - Atmos.* 108 (2003) 4447, doi:10.1029/2003JD003483.
- [77] J.J. Griffin, H. Windom, E.D. Goldberg, The distribution of clay minerals in the world ocean, *Deep-Sea Res.* 15 (1968) 433–459.
- [78] J.M. Prospero, E. Bonatti, Continental dust in the atmosphere of the eastern equatorial Pacific, *J. Geophys. Res.* 74 (1969) 3362–3371.
- [79] N. Mahowald, K. Kohfeld, M. Hansson, Y. Balkanski, S.P. Harrison, I.C. Prentice, M. Schulz, H. Rodhe, Dust sources and deposition during the last glacial maximum and current climate: a comparison of model results with paleodata from ice cores and marine sediments, *J. Geophys. Res. - Atmos.* 104 (1999) 15895–15916.
- [80] I. Farrera, S.P. Harrison, I.C. Prentice, G. Ramstein, J. Guiot, P.J. Bartlein, R. Bonnefille, M. Bush, W. Cramer, U. von Grafenstein, K. Holmgren, H. Hooghiemstra, G. Hope, D. Jolly, S.E. Lauritzen, Y. Ono, S. Pinot, M. Stute, G. Yu, Tropical climates at the Last Glacial Maximum: a new synthesis of terrestrial and palaeoclimate data: I. Vegetation, lake levels and geochemistry, *Clim. Dyn.* 15 (1999) 823–856.